

Mass loss from inhomogeneous hot star winds

III. An effective-opacity formalism for line radiative transfer in accelerating, clumped two-component media, and first results on theory and diagnostics

J.O. Sundqvist¹, J. Puls¹, and S.P. Owocki²

¹ Universitätssternwarte München, Scheinerstr. 1, 81679 München, Germany
e-mail: mail@jonsundqvist.com

² University of Delaware, Bartol Research Institute, Newark, Delaware 19716, USA

Received 2014-02-04; accepted 2014-05-27

ABSTRACT

Aims. To provide a fast and easy-to-use formalism for treating the reduction in effective opacity associated with optically thick clumps in an accelerating two-component medium.

Methods. We develop and benchmark effective-opacity laws for continuum and line radiative transfer that bridge the limits of optically thin and thick clumps. We then use this formalism to i) design a simple method for modeling and analyzing UV wind resonance lines in hot, massive stars, and ii) derive simple correction factors to the line force driving the outflows of such stars.

Results. Using a vorosity-modified Sobolev with exact integration (vmSEI) method, we show that, for a given ionization factor, UV resonance doublets may be used to analytically predict the upward corrections in empirically inferred mass-loss rates associated with porosity in velocity space (a.k.a. velocity-porosity, or vorosity). However, we also show the presence of a solution degeneracy: in a two-component clumped wind with given inter-clump medium density, there are *always* two different solutions producing the same synthetic doublet profile. We demonstrate this by application to SiIV and PV in B and O supergiants and derive, for an inter-clump density set to 1 % of the mean density, *upward empirical* mass-loss corrections of typically factors of either ~ 5 or ~ 50 , depending on which of the two solutions is chosen. Overall, our results indicate that this solution dichotomy severely limits the use of UV resonance lines as direct mass-loss indicators in current diagnostic models of clumped hot stellar winds.

We next apply the effective line-opacity formalism to the standard CAK theory of line-driven winds. A simple vorosity correction factor to the CAK line force is derived, which for normalized *velocity* filling factor f_{vel} simply scales as f_{vel}^α , where α is the slope of the CAK line-strength distribution function. By analytic and numerical hydrodynamics calculations, we further show that in cases where vorosity is important at the critical point setting the mass-loss rate, the reduced line force leads to a *lower theoretical* mass loss, by simply a factor f_{vel} . On the other hand, if vorosity is important only above this critical point, the predicted mass loss is not affected, but the wind terminal speed is reduced, by a factor scaling as $f_{\text{vel}}^{\alpha/(2-2\alpha)}$. This shows that porosity in velocity space can have a significant impact not only on the diagnostics, but also on the dynamics and theory of radiatively driven winds.

Key words. radiative transfer – techniques: spectroscopic – stars: early-type – stars: mass loss – stars: winds and outflows

1. Introduction

It has been known for several years now, that the powerful line-radiation driven winds of hot, massive stars are inhomogeneous and highly structured on small spatial scales (see overviews in Puls et al. 2008; Hamann et al. 2008; Sundqvist et al. 2012b). Such *wind clumping* arises naturally from the strong line-deshadowing instability – the LDI, a fundamental property of line driving (e.g., Owocki & Rybicki 1984, 1985) – and affects both theoretical models and the diagnostic radiative transfer tools needed to derive stellar and wind properties from observed spectra of massive stars. For example, neglect of clumping typically leads to observationally inferred mass-loss rates that differ by more than an order of magnitude for the same star, depending on which spectral diagnostic is used to estimate this mass loss (Fullerton et al. 2006).

Today’s diagnostic wind models normally account for inhomogeneities by simply assuming a one-component medium consisting of optically thin clumps of a certain volume filling factor (e.g., Hillier 1991; Puls et al. 2006). However, if individual clumps become optically thick, this leads to an additional leak-

age of light – not accounted for in the filling factor approach – through porous channels in between the clumps. Such porosity can occur either in the second and third spatial dimensions, or for spectral lines in *velocity-space* due to Doppler shifts in the rapidly accelerating wind (velocity-porosity, or “vorosity”, Owocki 2008). In Papers I and II of this series (Sundqvist et al. 2010, 2011), we developed detailed multi-dimensional wind models to study the effects of vorosity on the formation of, in particular, the strong UV “P-Cygni” lines that are the classical trademarks of massive star winds. A key general result from these studies is that clumps indeed easily become optically thick in such UV lines, and that the associated additional leakage of photons leads to weaker line profiles than predicted by smooth or volume filling factor models (see also Oskinova et al. 2007; Hillier 2008; Šurlan et al. 2012, 2013). But constructing realistic *ab-initio* radiation-hydrodynamic wind simulations that account naturally for spatial and velocity-field porosity is an extremely challenging and time-consuming task. Thus there is also a big need now for developing simplified, parameterized models that can be more routinely applied to diagnostic work on large samples of hot stars with winds, as well as be used to investigate gen-

eral effects on the theoretical predictions and dynamics of such winds. This paper develops such a simplified formalism, using effective quantities to simulate the reduction in opacity associated with optically thick clumps. In contrast to our earlier models (Sundqvist et al. 2010, 2011), this “effective opacity” approach has the great advantage that it can be readily implemented into the already existing NLTE (= non-local thermodynamic equilibrium) atmospheric models normally used to analyze observed spectra of hot stars with winds.

Sect. 2 develops and benchmarks effective-opacity laws to treat both continuum and line radiative transfer in accelerating, stochastic two-component media of (almost) arbitrary density contrasts. Sect. 3 then applies this effective opacity to line formation in hot stellar winds, investigating the influence of velocity-porosity on UV line diagnostics. Sect. 4 uses the same formalism to derive simple correction factors of the effects of such porosity on the line force driving the outflows of hot, massive stars, providing simple scaling relations for the effects on the global wind parameters mass-loss rate and terminal speed. Finally, Sect.5 summarizes main results and gives our conclusions.

2. Basic effective-opacity formalism

Although the primary aim of this paper is to develop a general and useful formalism for *line* opacity in accelerating, clumped two-component media, it is instructive to first consider the conceptually simpler case of *continuum* opacity. Below we present full effective-opacity bridging laws for such continuum absorption in a two-component medium with arbitrary density-contrast. This extends our previously developed “porosity models” (Owocki et al. 2004; Owocki & Cohen 2006; Sundqvist et al. 2012a), which have assumed one of the components to be effectively void, and also provides physical insights important for our following studies of line absorption.

2.1. Continuum absorption: A void interclump medium

Let us first very briefly review the case of an ensemble of clumps embedded in an effectively void “inter-clump medium”. For a given clump optical depth τ_{cl} and *mean* free path between clumps (a.k.a. the porosity length) h , the “effective” opacity (per unit length) is (e.g., Feldmeier et al. 2003; Owocki et al. 2004)

$$\chi_{\text{eff}} = \frac{1 - e^{-\tau_{cl}}}{h}. \quad (1)$$

Here $\tau_{cl} = \langle \chi \rangle h$, with mean opacity $\langle \chi \rangle$ and porosity length $h \equiv l_{cl}/f_{vol}$, with l_{cl} the characteristic length scale of clumps and f_{vol} the clump volume filling factor. Integrating the clump interaction probability $P = 1 - e^{-\tau_{cl}}$ over an exponential distribution in optical depths (or equivalently over l_{cl} , assuming a constant clump opacity),

$$f(\tau) = \frac{e^{-\tau/\tau_0}}{\tau_0}, \quad (2)$$

with

$$\langle \tau \rangle = \int_0^{\infty} \tau f(\tau) d\tau = \tau_0, \quad (3)$$

then gives the “inverse” bridging law for the effective opacity (Sundqvist et al. 2012a),

$$\frac{\chi_{\text{eff}}}{\langle \chi \rangle} = \frac{1}{1 + \tau_0} = \frac{1}{1 + \tau_{cl}}. \quad (4)$$

In this equation, $\langle \chi \rangle$ is the mean opacity calculated from a smooth model, or a structured model assuming optically thin clumps, and $\tau_0 = \tau_{cl} = \langle \chi \rangle h$ now represents the *mean* clump optical depth. In this paper, we assume this τ_{cl} is statistically isotropic. This results in an isotropic effective opacity (Sundqvist et al. 2012a), as favored by recent empirical investigations of X-ray line profile shapes in O-star winds (Leutenegger et al. 2013). Note that the porosity-associated reduction in effective opacity in this clump+void continuum model thus depends only on porosity length h .

2.2. Continuum absorption: Full bridging law for two-component media

Eqn. 4 above neglects absorption in the inter-clump (ic) medium. This is most probably a good assumption for continuum radiative transfer in stellar winds with clumping properties set by the LDI, but may be questionable for situations in which deep-seated atmospheric clumping might be expected, for example envelope inflation of stars that approach the Eddington limit (Gräfener et al. 2012; Gräfener & Vink 2013), or porosity-mediated continuum-driven mass loss in such stars (Owocki et al. 2004). We therefore next generalize the porosity model above to consider also the case where both components may contribute to the total opacity. For mean density $\langle \rho \rangle = f_{vol}\rho_{cl} + (1 - f_{vol})\rho_{ic}$, we approximate the opacity in such general two-component media with (see Appendix A)

$$\frac{\chi_{\text{eff}}}{\langle \chi \rangle} = \frac{1 + \tau_{cl}f_{ic}}{1 + \tau_{cl}}, \quad (5)$$

where $f_{ic} \equiv \rho_{ic}/\langle \rho \rangle$ denotes the contrast between inter-clump and mean density. Because of mass conservation, the clump optical depth for mass absorption coefficient κ and mean opacity $\langle \chi \rangle = \kappa\langle \rho \rangle$ now formally is

$$\tau_{cl} = \rho_{cl}\kappa l_{cl} = \langle \chi \rangle h \left(1 - (1 - f_{vol})f_{ic}\right), \quad (6)$$

however in most cases of interest the correction factor $1 - (1 - f_{vol})f_{ic}$ will be near unity, so that $\langle \rho \rangle \approx \rho_{cl}f_{vol}$ and $\tau_{cl} \approx \langle \chi \rangle h$ still are good approximations. We further note in this context that for processes with a density-independent mass absorption coefficient κ (like bound-free absorption of X-rays), the mean opacity $\langle \chi \rangle = \kappa\langle \rho \rangle$ is not directly affected by the presence of optically *thin* clumps, whereas for processes with $\kappa \propto \rho$ (like thermal free-free emission), this mean opacity is enhanced by a clumping factor $f_{cl} \equiv \langle \rho^2 \rangle / \langle \rho \rangle^2 \approx 1/f_{vol}$ (where the last approximation assumes a negligible contribution from the inter-clump medium) as compared to a homogeneous model.

To verify the bridging-law ansatz eqn. 5, we compare to an *exact* expression (derived analytically by Pomraning 1991, see also Levermore et al. 1986) for the emergent intensity in stochastic two-component media with spatially constant opacities and with length scales of the individual components distributed exponentially¹, as in our eqn. 2. Appendix A gives the formidable expression for this emergent intensity, along with a translation of the parameters used by Pomraning et al. to those used in this paper. Extensive testing comparing the analytic result with the simple bridging law eqn. 5 shows excellent agreement for a broad range of conditions, as illustrated by the opacity curves as functions of clump optical depth in the left hand panel of Fig. 1 (in which we also plot comparisons using a 3D-box

¹ Typically, such media are referred to as *Markovian binary mixtures*, see Pomraning (1991).

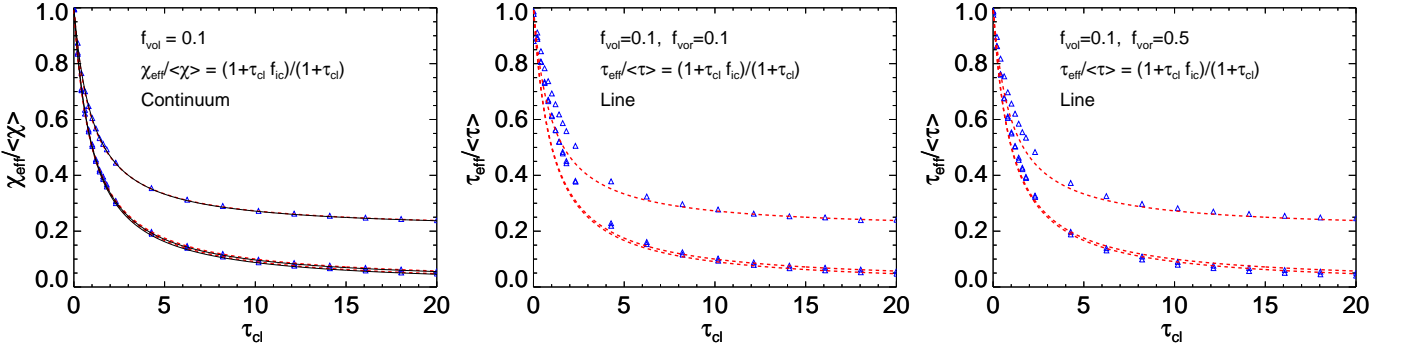


Fig. 1. Ratios of effective to mean opacity/optical depth for continuum absorption (left) and line absorption (middle, right), as functions of clump optical depth and for the parameters given in the panels and inter-clump density parameters $f_{ic} = 0, 0.01,$ and 0.2 (where the $f_{ic} = 0.2$ curve is the upper one in each panel). Note that the clump velocity span is $\delta v = \delta v_{sm}$ in the middle panel and $\delta v = 5\delta v_{sm}$ in the right one. Red dashed lines show the effective opacity/optical depth laws indicated in the figure, blue triangles show results from the 3D-box experiments described in the text, and the black solid lines in the left panel show the analytic expression given in Appendix A.

model, as described in the following subsection). We note in particular how previously known cases all are correctly reproduced by the new bridging law:

- optically thin clumps: $\tau_{cl} \ll 1 \rightarrow \chi_{eff} = \langle \chi \rangle$
- two equal components: $f_{ic} = 1 \rightarrow \chi_{eff} = \langle \chi \rangle$
- a negligible inter-clump medium density:
 $f_{ic} = 0 \rightarrow \chi_{eff} = \langle \chi \rangle / (1 + \tau_{cl})$ (eqn. 4).

Another interesting limit to examine is that of optically thick clumps and a tenuous but non-negligible inter-clump medium. In this case the product-term in eqn 5 decouples to yield $\chi_{eff}/\langle \chi \rangle \approx 1/\tau_{cl} + f_{ic}$. This simple expression illustrates explicitly how in the case of such black clumps the inter-clump medium may be viewed as gradually filling in the porous channels between the clumps. In contrast to the clump+void model, in which the opacity *itself* saturates at $\chi_{eff} = 1/h$ (and thus becomes independent of the mean opacity), in this general two-component model the *ratio* between the effective and mean opacities saturates, at $\chi_{eff}/\langle \chi \rangle = f_{ic}$ (see also Owocki et al. 2004). This means that, independent of the size of h , the medium can always become optically thick provided the mean opacity is high enough. Fig. 1 demonstrates that the opacity-ratio curve assuming a larger density contrast $f_{ic} = 0.01$ is almost indistinguishable from that assuming a void inter-clump medium, whereas the $f_{ic} = 0.2$ curve indeed approaches this $\chi_{eff}/\langle \chi \rangle \approx f_{ic}$ limit for very optically thick clumps.

2.3. Line absorption in rapidly accelerating media

Due to the Doppler effect, the formation of spectral lines in a clumped, accelerating medium differs conceptually from the continuum case studied above. Namely, for example in the supersonic, rapidly accelerating outflows of hot stars, each line photon can only interact with the wind material within a very narrow spatial range, set by the Sobolev length $L_{Sob} = v_{th}/v'$ for thermal speed v_{th} and velocity gradient v' . The small extent of this resonance zone makes it possible for line photons to leak through the wind via porous channels in velocity space, without ever interacting with the clumps. Hence we dub such leakage of light in velocity space *velocity-porosity*, or vorosity.

The clump optical depth in a spectral line. The difference between spatial porosity and velocity-porosity becomes particu-

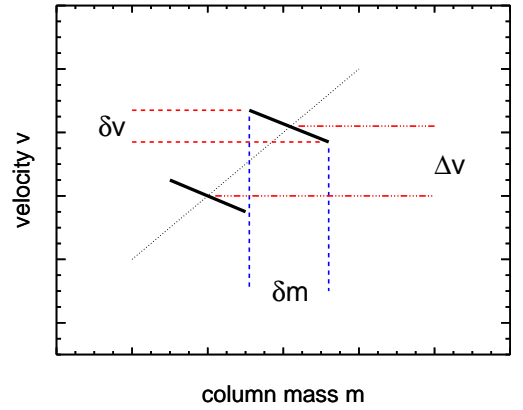


Fig. 2. Sketch of the vorosity effect in a model with clump column mass δm , clump velocity span δv , and mean velocity separation between clumps Δv . In the case of an inter-clump medium with negligible mass, all line photons with resonance frequencies that do not coincide with any velocities δv covered by the clumps will escape the wind without ever interacting with it, through the porous channels in velocity space set by $f_{vor} \equiv \delta v/\Delta v$. Note that in the special case of the radially compressed model discussed in text, $\delta m = \delta m_{sm}$, where δm_{sm} is the column mass contained within Δv in the initially smooth wind, which has here been swept up in the clump.

larly evident through the calculation of τ_{cl} . As for the continuum case, we in this paper take this line clump optical depth to be isotropic. Assuming then that the velocity span δv of individual clumps is greater than a few thermal widths ($v_{th} \approx 5-10$ km/s for a metal ion in a hot star wind), the clump optical depth of a spectral line, normalized in terms of the radial Sobolev optical depth τ_{Sob} in a smooth (sm) model (or one with optically thin clumps, if $\kappa \sim \rho$) can be written as

$$\frac{\tau_{cl}}{\tau_{Sob}} = \frac{\delta m}{\delta m_{sm}} \left| \frac{\delta v_{sm}}{\delta v} \right|, \quad (7)$$

where the δm 's and δv 's are the column masses and velocity spans of the clump and of the smooth wind, respectively. Note here that δm_{sm} and δv_{sm} as defined in eqn. 7 must be computed from the same length scale, but that the ratio $\delta v_{sm}/\delta m_{sm}$ (and thus the ratio τ_{cl}/τ_{Sob}) is independent of the choice of this scale.

In a first general model, we now *choose* δv_{sm} to be the velocity span a clump *would have* if it followed the smooth wind velocity law (so that $\delta m/\delta m_{\text{sm}} = \rho_{\text{cl}} l_{\text{cl}} / (\langle \rho \rangle l_{\text{cl}}) = \rho_{\text{cl}} / \langle \rho \rangle$), eqn. 7 can be further expressed as (see also Sundqvist et al. 2010, 2011)

$$\frac{\tau_{\text{cl}}}{\tau_{\text{Sob}}} = \frac{1}{f_{\text{vol}} |\delta v/\delta v_{\text{sm}}|} (1 - (1 - f_{\text{vol}}) f_{\text{ic}}) \approx \frac{1}{f_{\text{vol}} |\delta v/\delta v_{\text{sm}}|} = \frac{1}{f_{\text{vor}}}, \quad (8)$$

where the second expression here again neglects the small correction factor due to the inter-clump medium, and the third expression introduces the velocity clumping factor f_{vor} . This velocity clumping factor is defined as the ratio of the velocity span of clumps to their mean velocity separation Δv (see Fig. 2, and also Owocki 2008),

$$f_{\text{vor}} \equiv \left| \frac{\delta v}{\Delta v} \right|, \quad (9)$$

which is obtained in eqn. 8 by assuming clumps that, on average, have their central positions distributed in velocity-space according to the smooth wind expansion rate. In this case $\Delta v \approx v'_{\text{sm}} h$, using the definition of the porosity length $h \equiv l_{\text{cl}}/f_{\text{vol}}$ as the *mean* free path between clumps, which then results in $f_{\text{vol}} |\delta v/\delta v_{\text{sm}}| = (l_{\text{cl}}/h) |\delta v/(v'_{\text{sm}} l_{\text{cl}})| = |\delta v/\Delta v| = f_{\text{vor}}$.

While eqn. 8 is a quite general expression for τ_{cl} , a conceptually better understanding of how f_{vor} determines the velocity-porosity effect can be obtained by considering a simple model of radially compressed clumps consisting of swept up material from an initially smooth wind (similar to predictions of present-day LDI simulations). For this model then (see sketch in Fig. 2), the initially smooth wind contained within Δv will have a column mass $\Delta m = \delta m_{\text{sm}} = \delta m$, so that

$$\frac{\tau_{\text{cl}}}{\tau_{\text{Sob}}} = \frac{\delta m}{\delta m_{\text{sm}}} \left| \frac{\delta v_{\text{sm}}}{\delta v} \right| = \left| \frac{\Delta v}{\delta v} \right| = \frac{1}{f_{\text{vor}}}. \quad (10)$$

Moreover, we can of course also in this model choose to instead define the smooth wind quantities on the clump length scale, so that in this case $\delta v = (\delta v/\delta v_{\text{sm}}) v'_{\text{sm}} l_{\text{cl}}$ and, since the mean free path between clumps in Fig. 2 still is $h = \Delta v/v'_{\text{sm}}$, the velocity clumping factor $f_{\text{vor}} = f_{\text{vol}} |\delta v/\delta v_{\text{sm}}|$. This shows that this one-dimensional radially compressed model is fully consistent with the more general eqn. 8. Note also that f_{vor} as defined here is an *un-normalized* quantity, which only for the case that the velocity field inside the clumps follows the smooth wind velocity law becomes a normalized quantity.

In summary, the key point is that the final expression for the clump optical depth depends *only* on this velocity clumping factor (and a correction factor for the mass contained in the inter-clump medium).

Effective opacity bridging law for spectral lines. For line clump optical depth $\tau_{\text{cl}} = \tau_{\text{Sob}}/f_{\text{vor}} \times (1 - f_{\text{ic}}(1 - f_{\text{vol}})) \approx \tau_{\text{Sob}}/f_{\text{vor}}$, we now (in analogy with the continuum case) suggest to write the vorosity-modified effective line opacity as

$$\frac{\chi_{\text{eff}}}{\langle \chi \rangle} = \frac{1 + \tau_{\text{cl}} f_{\text{ic}}}{1 + \tau_{\text{cl}}}, \quad (11)$$

where the correction factor $\tau_{\text{cl}} f_{\text{ic}}$ in the nominator now essentially assumes that the inter-clump medium, on average, follows the smooth wind expansion rate, and so fills in all holes in velocity space not covered by the dense clumps. This simple treatment of the inter-clump medium allows us to account for the fact that UV line profiles in dense O-star winds often exhibit zero

residual flux (in particular at high velocities), which is direct observational evidence that at least some material must be present at a wide range of wind velocities (e.g., Sundqvist et al. 2010). Another inherent assumption in eqn. 11, retained throughout this paper, is that the ionization states of the two components of the medium can be approximated with one “effective” state (for a first attempt to build a two-component model that relaxes this, see Zsargó et al. 2008).

Eqn. 11, like the continuum opacity bridging law, gives the expected results in previously studied limits, namely:

- optically thin clumps: $\tau_{\text{cl}} \ll 1 \rightarrow \chi_{\text{eff}} = \langle \chi \rangle$
- two equal components: $f_{\text{ic}} = 1 \rightarrow \chi_{\text{eff}} = \langle \chi \rangle$
- optically thick clumps and a negligible inter-clump medium: $f_{\text{ic}} = 0 \tau_{\text{cl}} \gg 1 \rightarrow \tau_{\text{eff}} = \chi_{\text{eff}}/v'_{\text{sm}} = f_{\text{vor}}$,

where the last limit is valid for rays in the radial direction and illustrates how we perform the final radiative transfer calculations on a background smooth model, which is the simplifying key point in developing this kind of effective-opacity formalisms. The limit shows further how in the absence of an infilling inter-clump medium, the effective line optical depth in the radial direction saturates at a value given simply by f_{vor} , which means that the escape fraction of line photons in this case is $e^{-f_{\text{vor}}}$. Physically, this is analogous to the escape fraction of light in traditional radiative transfer models, but with the spatial holes between randomly distributed atomic absorbers replaced here by velocity holes between clumps that are randomly distributed about their mean in velocity space (see also discussion in Sundqvist et al. 2011, their Appendix A). Since $f_{\text{vor}} = 1$ still gives an escape fraction e^{-1} , this property shows the importance of defining f_{vor} as an *un-normalized* quantity (not bound between 0 and 1) in such effective-opacity models, so that optically thick conditions with $f_{\text{vor}} \rightarrow \infty$ can be reached.

It is, finally, important to realize that although the proposed continuum and line effective-opacity laws have the same principal forms, the conceptual difference between spatial porosity and velocity-porosity is reflected in the calculation of the clump optical depth, which for continuum opacity depends on porosity length h , and for line opacity on velocity clumping factor f_{vor} .

Benchmarking with 3D-box experiments. Before considering the specific case of line formation in rapidly accelerating stellar winds, we first test the general validity of the new bridging law. For this purpose, we randomly distribute clumps in a 3D-box according to (constant) pre-specified volume filling factors, clump length scales, and opacities for both clumps and the inter-clump medium. For each such randomization, a ray is fired from the bottom of the box and the emergent intensity I computed at the top. This procedure is then repeated until statistical errors in the averaged intensities are sufficiently small, resulting in a final effective optical depth $\tau_{\text{eff}} = -\ln \langle I \rangle$. For clump length scales distributed exponentially according to eqn. 2, we have verified that for continuum opacity this set-up gives perfect agreement with the analytic expression provided in Appendix A (and thus also with the continuum effective-opacity bridging law), as illustrated by the blue triangles in the left hand panel of Fig. 1.

To study line formation, we add to the continuum set-up a simple velocity field proportional to height Z in the box, and evaluate the Sobolev optical depth at the points where a given line-frequency has been Doppler shifted into resonance (which can be more than one due to the random distribution of clumps). We assign an inter-clump optical depth τ_{ic} only to rays that do not intersect any clump. This effectively assumes an inter-clump

medium density $\rho_{ic}/\langle\rho\rangle \lesssim 0.2$, so that clumps still dominate the total absorption whenever they are intersected. To facilitate comparisons, we re-formulate eqn. 11 in terms of the vorosity-modified effective optical depth²

$$\frac{\tau_{\text{eff}}}{\langle\tau\rangle} \approx \frac{\tau_{\text{eff}}}{\tau_{\text{Sob}}} = \frac{1 + \tau_{\text{cl}}f_{\text{ic}}}{1 + \tau_{\text{cl}}}. \quad (12)$$

The middle and right hand panels of Fig. 1 compare effective optical depth curves of the line-opacity bridging law to the 3D box simulations, and show an overall good agreement. Whereas the middle panel assumes a velocity span of clumps δv that follows the underlying mean expansion δv_{sm} , the right panel shows that the bridging law is valid also for velocity spans that deviate from this expansion rate, here using $\delta v = 5\delta v_{\text{sm}}$; since the opacity curves in the two panels are plotted against the clump optical depth $\propto \tau_{\text{Sob}}/f_{\text{vor}}$, they automatically adjust for the different assumed velocity filling factors and so appear similar in the figure. As in the continuum case, the figure shows that the effective optical depth approaches $\langle\tau_{\text{eff}}\rangle/\tau_{\text{Sob}} \approx f_{\text{ic}}$ for very optically thick clumps. In summary, these 3D box experiments thus provide good general support for the proposed effective-opacity bridging law to treat line opacity in a rapidly accelerating, stochastic two-component medium.

Backed up by these results, we next consider two applications of the effective-opacity bridging law developed in this section, namely: i) a very simple method for computing and analyzing UV resonance lines from the winds of hot, massive stars, and ii) an equally simple method for estimating the vorosity effect on the driving line force of such winds.

3. Application I: Line diagnostics

The standard Sobolev with exact integration (SEI, Lamers et al. 1987) method for computing UV wind resonance lines uses the Sobolev approximation to first obtain the source function, after which the formal integral of radiative transfer is solved exactly to compute the emergent flux spectrum. This section first develops a simple vorosity-modified SEI method (vmSEI), by using the effective-opacity bridging law introduced above, and then demonstrates how it may be analytically applied to obtain vorosity corrections for empirically inferred mass-loss rates.

3.1. A vorosity-modified SEI method

The opacity of a trace element in a UV wind resonance line can, for mass-loss rate \dot{M} and wind terminal speed v_{∞} , ion fraction q of the considered element i , and abundance with respect to hydrogen $\alpha_i = n_i/n_{\text{H}}$, be conveniently expressed as a dimensionless opacity-parameter (Hamann 1981)

$$\kappa_0 = \frac{\dot{M}q}{R_{\star}v_{\infty}^2} \frac{\pi e^2/m_e c}{4\pi m_{\text{H}}} \frac{\alpha_i}{1 + 4Y_{\text{He}}} f_{\text{lu}}\lambda_0, \quad (13)$$

where it has been assumed that the entire ion population resides in the ground state (normally a safe assumption for the lines considered in this paper, e.g. Puls et al. 2008). In eqn. 13, R_{\star} is the

² The mean optical depth in the random-box experiment can be computed from the specific probabilities that a clump or the inter-clump medium is hit. After integrating over an exponential distribution in clump length scales, this results in $\langle\tau\rangle = f_{\text{vor}}/(1 + f_{\text{vor}})\tau_{\text{cl}} + 1/(1 + f_{\text{vor}})\tau_{\text{ic}}$. Accounting additionally for the fact that more than one clump can be hit due to overlaps in velocity space, we approximate $\langle\tau\rangle \approx f_{\text{vor}}\tau_{\text{cl}} + 1/(1 + f_{\text{vor}})\tau_{\text{ic}} = \tau_{\text{Sob}}(1 + f_{\text{ic}}/(1 + f_{\text{vor}})) \approx \tau_{\text{Sob}}$ for the $f_{\text{ic}} \lesssim 0.2$ considered here.

stellar radius, Y_{He} the helium number abundance, f_{lu} the oscillator strength of the transition, and λ_0 the rest wavelength. With this parametrization, the radial Sobolev optical depth in a smooth wind becomes

$$\tau_{\text{Sob}}(r) = \frac{\kappa_0}{r^2 w dw/dr}, \quad (14)$$

where r is measured in units of R_{\star} and $w = v/v_{\infty}$. To account for the effects of optically thick clumping, we now simply replace the opacity parameter κ_0 with the radius dependent (but angle independent) effective opacity

$$\kappa_{\text{eff}}(r) = \left(\frac{1 + \tau_{\text{cl}}f_{\text{ic}}}{1 + \tau_{\text{cl}}} \right) \kappa_0. \quad (15)$$

For pre-specified velocity clumping factor f_{vor} and inter-clump medium density parameter f_{ic} , implementing eqn. 15 in a SEI code thus reduces to evaluating the clump optical depth $\tau_{\text{cl}}(r) = \tau_{\text{Sob}}/f_{\text{vor}} \times (1 - (1 - f_{\text{vor}})f_{\text{ic}}) \approx \tau_{\text{Sob}}/f_{\text{vor}}$ at each radial grid point. Using the obtained effective opacity the source functions are then calculated from the angle dependent effective Sobolev optical depth $\tau_{\text{eff}}^{\text{Sob}}(r, \mu) = \kappa_{\text{eff}}/(r^2 w Q)$, with $Q \equiv \mu^2 dw/dr + (1 - \mu^2)w/r$ for directional cosine μ , and the formal integral finally solved following the standard SEI approach.

For a modestly overlapping resonance doublet and a standard wind velocity law³ $w = (1 - 0.99/r)^{\beta}$, here with $\beta = 1$, the two leftmost panels of Fig. 3 compare line profiles computed using this vmSEI approach with profiles computed using the standard SEI model, for intermediate and strong lines with $\kappa_0 = 1$ and 100. The figure shows clearly the basic velocity-porosity effect, namely weaker line-profiles for a given line-strength parameter κ_0 , consistent with all previous work on the effects of optically thick clumps on UV wind lines (Oskinova et al. 2007; Sundqvist et al. 2010, 2011; Šurlan et al. 2012, 2013).

Moreover, for the models with void inter-clump medium the absorption in the lines saturates at a level above zero, at $\sim e^{-f_{\text{vor}}}$ (as discussed in Sect. 2.3), whereas in the case of $f_{\text{ic}} = 0.1$ the strong $\kappa_0 = 100$ line recovers the absorption blackness of the smooth model. Another important result of vorosity evident from the figure, is that the relative strength between the blue and red components can differ significantly from the expected factor of 2 in optical depth (stemming from the oscillator strength ratio, see also Prinja & Massa 2010; Sundqvist et al. 2011; Prinja & Massa 2013); this last property is examined in detail in Sect. 3.3.

3.2. Comparison to Monte-Carlo simulations

We next compare this new vmSEI model to profiles computed using an extension (to treat doublets) of the method developed by Sundqvist et al. (2010). This creates a multi-dimensional stochastic wind by taking 1-D snapshots and phasing them randomly in patches of a parameterized angular size, here 3 degrees, and then computes synthetic spectra via a Monte-Carlo radiative transfer technique. These stochastic wind models are created such that they preserve the basic properties of LDI simulations, while still allowing for different quantitative wind structure properties by the adjustment of a number of input parameters, as given by Table 1. In the test cases displayed in Fig. 3, we have assumed a ‘‘velocity-stretch’’ porosity law (e.g., Sundqvist et al. 2012a) $h/R_{\star} = w$, a clump onset radius $r_{\text{cl}} = 1.1R_{\star}$, and shock jump velocity $v_j = 0.1w$, where the shock

³ 0.99 corresponds to $v_{\text{min}} = 0.01v_{\infty}$ for a $\beta = 1$ velocity field.

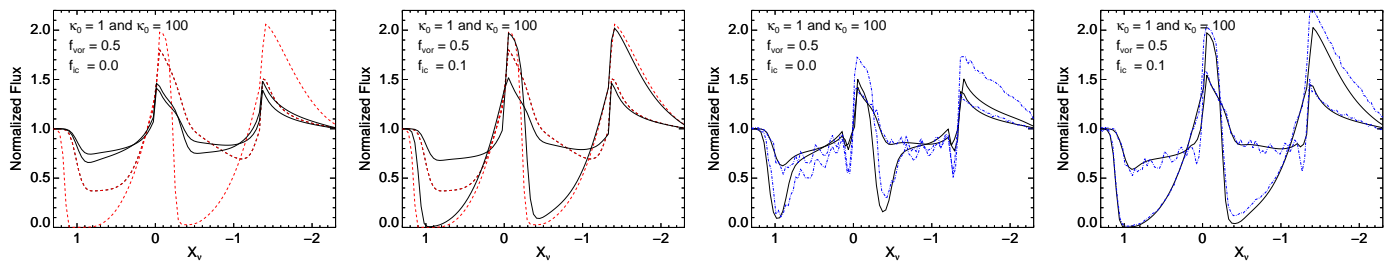


Fig. 3. Synthetic UV line profiles in units of normalized frequency $X_v = (v/v_0 - 1)c/v_\infty$, and for velocity separation $v_{\text{sep}}/v_\infty = 1.35$ between the line-centers of the two doublet components (which corresponds to the separation of the PV resonance doublet in a wind with $v_\infty = 2000$ km/s). For the line-strengths and clumping parameters indicated in the panels and described in table 1 and in text, the black lines show profiles computed using the vmSEI method developed here, the red dashed lines (two leftmost panels) show results from the standard SEI method (assuming a smooth wind), and the blue dashed lines (two rightmost panels) show results from the Monte-Carlo method by Sundqvist et al. (2010). Note that the velocity clumping factors indicated in the panels are based on the original definition eqn. 9 rather than the modified eqn. 16.

Table 1. Input parameters in the Monte-Carlo, multi-dimensional, stochastic wind simulations by Sundqvist et al. (2010, 2011).

Parameter	Clump volume filling factor	Clump velocity span	Porosity length	Inter-clump density parameter	Shock jump velocity
Symbol	f_{vol}	$ \delta v/\delta v_{\text{sm}} $	h	f_{ic}	v_j

jump velocity in the vmSEI model is simulated using the same “turbulent” velocity parameter v_{turb} as in the traditional SEI approach. The rightmost two panels of Fig. 3 show an overall good agreement between the two methods, providing general support for the usage of the much simpler effective-opacity method for the quantitative analysis of hot stellar wind spectra.

One feature in the stochastic models not captured by the vmSEI approach is the redward excess emission in strong lines. This excess is caused by photon trapping within the resonance zones and by increased back-scattering due to multiple such resonance zones (Lucy 1984; Puls et al. 1993; Sundqvist et al. 2010), which allows light to escape primarily when emitted on the red side of the line profile; such multi-scattering effects cannot be simulated within the simple effective opacity method developed in this paper, but does not affect the *absorption* line strength that is the primary focus here (and in general when using unsaturated resonance lines as diagnostic tools). Moreover, in particular the $\kappa_0 = 100$ line with a void inter-clump medium shows a prominent absorption-dip towards the blue edge of the profile (see also Sundqvist et al. 2010; Šurlan et al. 2012). In the stochastic wind models, overlapping clumps in velocity space and the finite extent of the line profile lead to an increase in f_{vor} at high velocities, and so results in more efficient absorption in the outermost wind than in the accelerating parts of it. To account for this absorption effect in the vmSEI model, we re-write the velocity clumping factor as (Sundqvist et al. 2011, their Appendix A)

$$f_{\text{vor}} \approx \left| \frac{\delta v + v_{\text{th}}}{\Delta v} \right| = f_{\text{vol}} \left| \frac{\delta v}{\delta v_{\text{sm}}} \right| + \frac{L_{\text{Sob}}}{h}. \quad (16)$$

This equation shows that, for a given inter-clump density, the other vorosity-related input parameters in the stochastic wind models (see Table 1) can be combined into one, the velocity clumping factor f_{vor} . It also demonstrates how the absorption-dips in the stochastic models result from the very large Sobolev lengths in the outermost wind, which give the radiative transfer a pseudo-continuum character that reduces the velocity-porosity effect (which requires rapid acceleration). In this respect, we note also that the Monte-Carlo calculations performed

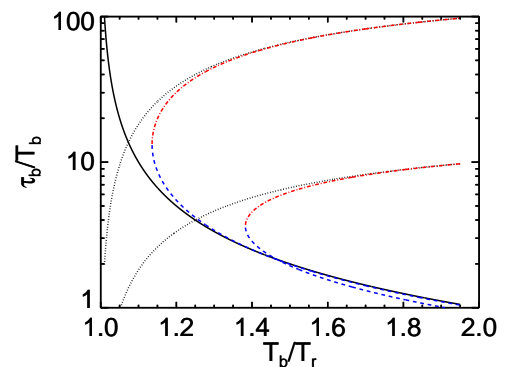


Fig. 4. vmSEI optical depth correction factors τ_b/T_b as function of fiducial resonance doublet optical depth ratio T_b/T_r . The black solid and dotted lines are computed using eqns. 20 and 24, and the blue dashed and red dashed-dotted lines show the two solution branches from solving eqn.22 for inter-clump density parameters $f_{\text{ic}} = 0.01$ and 0.1.

by Sundqvist et al. (2011) directly on LDI simulations confirm that the dip is present also in such hydrodynamical wind models calculated from first principles.

It is important to realize here, however, that using f_{vor} as an empirical input-parameter when calculating the effective opacity, or as a fit parameter when modeling observed line profiles, *automatically* accounts for this outer-wind absorption effect (if present).

We next demonstrate how, indeed, unsaturated resonance doublets can be used to directly diagnose the radial behavior of the velocity filling factor, as well as to derive vorosity corrections for empirically inferred mass-loss rates.

3.3. An analytic method for vorosity mass-loss corrections

As first pointed out in the context of hot star winds by Massa et al. (2008), in a homogeneous (or optically thin clumped) wind the optical depths of the individual components

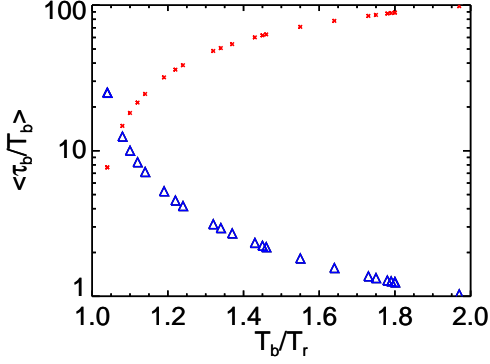


Fig. 5. The two solution branches for vmSEI mass loss times ion correction factors for the B supergiant sample of Prinja & Massa (2010) and inter-clump density parameter $f_{ic} = 0.01$ (see text).

of a resonance doublet must be set by the ratio of their oscillator strengths. On the other hand, in a wind consisting of some mixture of thin and thick clumps (and a potentially non-void inter-clump medium), this is no longer necessarily the case. By allowing the oscillator strength ratio in the standard SEI model to be a free parameter (or alternatively examining only completely separated doublets, see Prinja & Massa 2010, 2013), we can empirically infer “fiducial” Sobolev optical depths T_b and T_r for the blue and red components. We show below how these fiducial optical depths derived from a *smooth* wind model then can be used to analytically obtain f_{vor} and correction factors to the product of mass-loss rate and ion fraction.

A void inter-clump medium. Neglecting first absorption within a tenuous inter-clump medium, we demand that T_b and T_r be equal to the vorosity-modified effective optical depths,

$$T_b = \tau_{\text{eff}}^b = \frac{\tau^b}{1 + \tau^b/f_{\text{vor}}}, \quad (17)$$

$$T_r = \tau_{\text{eff}}^r = \frac{\tau^b/2}{1 + \tau^b/(2f_{\text{vor}})}, \quad (18)$$

where for simplicity we have denoted the Sobolev optical depth by τ , and, of course, in the physics-based vorosity model the *real* oscillator strength ratio f_b/f_r must be used; to allow for an analytic investigation, we here assume $f_b/f_r = 2$, which is true for most UV resonance lines of interest (for example PV, CIV, SiIV). For given T_r and T_b then, we thus have two equations and two unknowns and can solve immediately for the velocity clumping factor and the vorosity correction in optical depth,

$$f_{\text{vor}} = T_b \frac{1}{2 - T_b/T_r}, \quad (19)$$

$$\frac{\tau^b}{T_b} = \frac{(\dot{M}q)_{\text{vmSEI}}}{(\dot{M}q)_{\text{SEI}}} = \frac{1}{T_b/T_r - 1}. \quad (20)$$

All quantities in these equations are *local*, i.e., by scanning the observed line profile one finds T_b and T_r as a function of radius and so also $f_{\text{vor}}(r)$ and the optical depth correction $(\tau_b/T_b)(r)$.

Analysis of the remarkably simple eqns. 19 and 20 shows that in the physical limit $T_b/T_r \rightarrow 2$, the vorosity mass-loss (times ion fraction) correction goes to unity and $f_{\text{vor}} \rightarrow \infty$; this is expected since in this case the smooth wind conditions should be recovered, and in this clump+void model the only way to achieve

this is by making all clumps optically thin, i.e. $\tau_{\text{cl}} = \tau/f_{\text{vor}} \rightarrow 0$, which requires $f_{\text{vor}} \rightarrow \infty$. In the opposite limit $T_b/T_r \rightarrow 1$, the mass-loss correction approaches ∞ and $f_{\text{vor}} \rightarrow T_b$; such huge mass-loss correction for this case is also as expected, since we showed in Sect. 2.3 that in this limit $\tau_{\text{eff}} = f_{\text{vor}}$, and the profile-strength then becomes *independent* of mass loss.

We note also that while the velocity clumping factor depends on the actual empirically inferred profile strength T_b , the quantity τ_b/T_b depends *only* on the ratio T_b/T_r . This very simple property makes it particularly appealing to consider the behavior of such vorosity corrections for mass loss, which we indeed focus on in the analysis below.

Adding an absorbing inter-clump medium. Adding a non-void inter-clump medium that contributes to the total opacity gives for the equations to be solved,

$$T_b = \tau_{\text{eff}}^b = \frac{\tau^b + (\tau^b)^2 f_{ic}/f_{\text{vor}}}{1 + \tau^b/f_{\text{vor}}}, \quad (21)$$

$$T_r = \tau_{\text{eff}}^r = \frac{\tau^b/2 + (\tau^b)^2 f_{ic}/(4f_{\text{vor}})}{1 + \tau^b/(2f_{\text{vor}})}. \quad (22)$$

For given f_{ic} this is now a quadratic system with two distinct solution branches. It is readily solved by any mathematical software package, but the solutions are too complex to be given explicitly here. For a given f_{ic} , real-valued roots exist above a given T_b/T_r threshold, as illustrated by Fig. 4. The blue dashed curves in Fig. 4 further show that for physically reasonable values $f_{ic} \lesssim 0.1$, the first solution branch is characterized by simply a small correction factor to the previous expression (eqn. 20) neglecting f_{ic} . But as also seen from the figure (the red dashed-dotted curves), the other solution branch represents fundamentally different values of mass-loss corrections. We can understand this by considering the limiting case of optically thick clumps and a tenuous inter-clump medium, for which the bridging law above can be approximated with $\tau_{\text{eff}} \approx f_{\text{vor}} + f_{ic}\tau$, resulting in

$$f_{\text{vor}} = T_r(2 - T_b/T_r), \quad (23)$$

$$\frac{\tau^b}{T_b} = \frac{(\dot{M}q)_{\text{vmSEI}}}{(\dot{M}q)_{\text{SEI}}} = \frac{2(1 - T_r/T_b)}{f_{ic}}. \quad (24)$$

This solution now offers a second possibility, in addition to eqn. 20, to recover the smooth wind results as $T_b/T_r \rightarrow 2$, namely by absorption within the inter-clump medium. The scaling of mass-loss correction now is $\sim 1/f_{ic}$, as illustrated by the black dotted curves in Fig. 4. Physically, this scaling comes from the fact that almost all absorption now takes place in the inter-clump medium that fills the velocity-gaps between dense clumps, which for typical values $f_{ic} \approx 0.01$ can lead to *very* large mass-loss corrections.

The two branches thus represent real solution degeneracies in the two-component clumped models, physically characterized by absorption in either i) a mixture of optically thin and thick clumps, or ii) optically thick clumps where the velocity gaps are being filled in by the inter-clump medium. Calculations using the vmSEI model confirm that line profiles from the two solution branches are indeed identical. This essentially implies that when using resonance doublets as diagnostic tools in a two-component clumped wind, there will always be two possibilities to reproduce the same line-profile doublet, even if one invokes additional constraints (either theoretical, or from alternative diagnostics) about the inter-clump medium.

3.4. Vorosity mass-loss correction of Si IV in B supergiants

Prinja & Massa (2010) derived T_b/T_r ratios (averaged within $0.2v_\infty \leq v \leq 0.8v_\infty$) for a sample of B-supergiants using the well separated Si IV doublet. We here simply take their derived ratios and apply the formalism developed above to obtain the vorosity corrections for mass loss times ion fraction. Since individual values for T_b and T_r are not provided by Prinja & Massa, we do not derive corresponding values for f_{vor} in this subsection. For the supersonic wind, LDI simulations typically predict a very tenuous inter-clump medium, on order $f_{\text{ic}} \approx 0.01$, allowing us to use the simplified eqns. 20 and 24 for the analysis here (instead of the more complicated full solution to eqn. 22). We further neglect stars in the sample with unphysically derived values, i.e. those few stars with $T_b/T_r > 2$ or $T_b/T_r < 1$. Fig. 5 shows our result, giving for the first solution branch a reasonable average factor of ~ 5 for the upward mass loss correction factor. The same analysis for the second solution branch gives an average scaling $\sim 50/f_{\text{ic}}^{0.01}$, with the inter-clump medium density parameter measured in units of our standard choice 0.01. The results also reveal a large scatter about the mean, indicating that the clumping properties of such B supergiants may vary quite significantly from star to star.

3.5. Vorosity mass-loss corrections of PV in ζ Pup and λ Cep

Using observed spectra from *Copernicus* and *FUSE* (Fullerton et al. 2006), we next perform explicit line-profile fitting of the unsaturated phosphorus V (PV) resonance doublet at $\lambda\lambda 1118, 1128$ in the prototypical Galactic O supergiants ζ Pup, O4I(n)f, and λ Cep, O6I(n)fp. Using $\beta = 0.7$ (λ Cep) and $\beta = 0.5$ (ζ Pup) velocity laws (Fullerton et al. 2006)⁴, we first use a normal SEI model with line-strength κ_0 and the oscillator strength ratio $f_b/f_r = T_b/T_r$ in 20 discrete velocity bins of $0.05v_\infty$ each as free input parameters. After a simple χ^2 minimization, the obtained best-fit parameters are translated to velocity clumping factors and new values for the line-strength κ_0 according to the method outlined in previous subsections.

Focusing first on ζ Pup, the left panel in Fig. 6 shows profile fits for the two solution branches of the vmSEI model (black solid and blue dashed lines), and a comparison best-fit smooth-wind model with a fixed oscillator strength ratio 2 (black dotted line). We note from the figure that the vmSEI model fits still are not perfect; indeed, a completely perfect fit to the observed *Copernicus* line spectrum would in some velocity bins require values of $f_b/f_r = T_b/T_r$ above 2 or below 1, translating then to unphysical values of the velocity filling factor. Nonetheless, the vmSEI model is a clear improvement over the standard smooth-wind SEI fit. The black solid and blue dashed curves illustrate the degenerate results from the two solution branches, here again assuming $f_{\text{ic}} = 0.01$. Averaged over velocity bins within $0.3v \leq v_\infty \leq 0.8v$, the first solution results in a mass-loss times PV ion fraction correction factor for ζ Pup of $\langle \dot{M}q \rangle_{\text{vmSEI}} / \langle \dot{M}q \rangle_{\text{SEI}} = 6$, and a *normalized velocity filling factor*

$$f_{\text{vel}} \equiv \frac{\delta v}{\delta v + \Delta v} = \frac{f_{\text{vor}}}{1 + f_{\text{vor}}}, \quad (25)$$

of $\langle f_{\text{vel}} \rangle = 0.65$. The second solution displayed in the figure, however, has a *much* higher $\langle \dot{M}q \rangle_{\text{vmSEI}} / \langle \dot{M}q \rangle_{\text{SEI}} = 60$, and correspondingly a lower $\langle f_{\text{vel}} \rangle = 0.2$. As discussed in the previous subsection, the mass-loss corrections from such second

⁴ A velocity field exponent $\beta = 0.5$ indeed seems somewhat low, but assuming such steep wind acceleration actually provides the best fits to the shapes of the PV lines in ζ Pup.

branch solutions are further scalable in f_{ic} , here according to $\langle \dot{M}q \rangle_{\text{vmSEI}} / \langle \dot{M}q \rangle_{\text{SEI}} \approx 60 / f_{\text{ic}}^{0.01}$.

For λ Cep (the right panel in Fig. 6), the first solution branch gives a very modest 20 % upward correction in mass loss times ion fraction, accompanied by a high $\langle f_{\text{vel}} \rangle = 0.81$. Note further that the best-fit here is almost indistinguishable from that using the SEI smooth-wind model with a fixed $f_b/f_r = 2$; this is because the line-strength ratio of the PV blue to red components in λ Cep corresponds almost to a factor of two in optical depth, which leaves essentially no room for velocity-porosity on the first solution branch (see Fig. 4). On the other hand, using the second solution tree again results in equally good fits (see the dashed blue line), and in large mass-loss corrections $\langle \dot{M}q \rangle_{\text{vmSEI}} / \langle \dot{M}q \rangle_{\text{SEI}} = 90 / f_{\text{ic}}^{0.01}$, as well as a very low velocity filling factor $\langle f_{\text{vel}} \rangle = 0.04$ for the standard case $f_{\text{ic}} = 0.01$.

Physically, these results again reflect the fact that in a two-component clumped stellar wind, there are two possibilities of obtaining the same line profile: either by absorption in moderately optically thick clumps (with clump optical depths reflected in the observed line-strength ratio), or by filling in the velocity-gaps between optically thick clumps (which shifts the line-strength ratio – which *always* is unity for such optically thick clumps – to that observed).

It is tempting here to argue that the first solution branch is the physically more viable, since the inter-clump densities $f_{\text{ic}} \sim 0.01$ typical of LDI wind simulations otherwise would lead to very large, ~ 100 , upward corrections in mass loss. As shown above, applying the first solution for ζ Pup leads to a factor of ~ 6 in upward correction of the smooth wind mass-loss rate times PV ion fraction. Applying this to the PV rate obtained by Fullerton et al. (2006) results in $\langle q \rangle_{\text{PV}} \dot{M} \approx 2.6 \times 10^{-6} M_\odot/\text{yr}$, which for $\langle q \rangle_{\text{PV}} \approx 0.5 - 1$, as predicted by present day NLTE atmosphere codes like *FASTWIND* (Puls et al. 2005), gives a rate in good agreement with other recent mass loss determinations of this star (Najarro et al. 2011; Bouret et al. 2012; Šurlan et al. 2013; Hervé et al. 2013; Cohen et al. 2014).

But as discussed above, for λ Cep this solution leads to only a modest 20 % upward correction, which (again using the results of Fullerton et al. 2006) yields $\langle q \rangle_{\text{PV}} \dot{M} \approx 0.3 \times 10^{-6} M_\odot/\text{yr}$. Since $\langle q \rangle_{\text{PV}} \approx 0.5 - 1$ is predicted also for this star, this would imply a very low mass-loss rate, a factor of several lower than that derived from similar velocity-porosity models by Sundqvist et al. (2011) (who essentially ignored the additional information contained in the doublet-*ratio*) and by Šurlan et al. (2013). Indeed, the rate obtained by the latter authors corresponds to the second solution branch found in this paper, which for their very high assumed $f_{\text{ic}} = 0.15$ gives a correction factor ~ 5 for λ Cep and $\langle q \rangle_{\text{PV}} \dot{M} \approx 1.4 \times 10^{-6} M_\odot/\text{yr}$. This is in good agreement with the $\dot{M} = 1.6 \times 10^{-6} M_\odot/\text{yr}$ obtained from the independent models by Šurlan et al. (2013). (Actually, also the rate these authors obtain for ζ Pup corresponds to the second branch solution; their $\dot{M} = 2.5 \times 10^{-6} M_\odot/\text{yr}$ for $f_{\text{ic}} = 0.15$ again agrees well with the rate derived in the analysis above when assuming the second branch solution.) In Sect. 5, we further discuss consequences of these severe degeneracies when empirically deriving mass-loss rates from UV wind lines.

4. Application II: Line-driven wind theory

Having analyzed in detail how velocity-porosity affects UV spectral line diagnostics, we next examine the related question of how such vorosity might affect the line force driving the outflows of hot, massive stars.

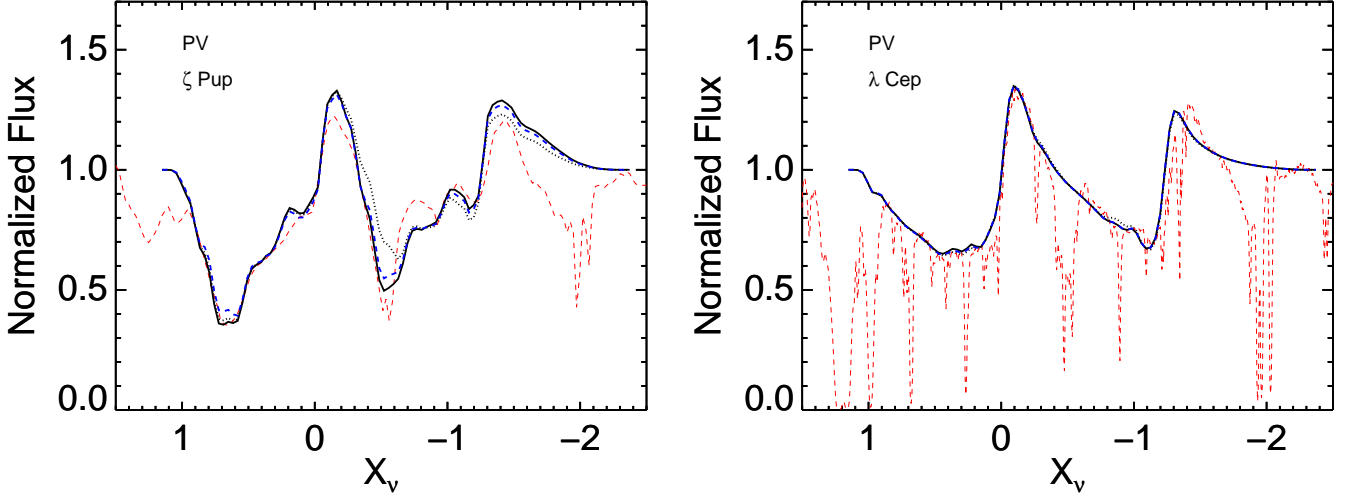


Fig. 6. Observed and modeled PV spectra of ζ Pup, observations from *Copernicus*, and λ Cep, observations from *FUSE*. Black solid and blue dashed lines are vmSEI model fits from the first and second solution branches, respectively (see text), the dotted black lines are fits from a smooth-wind model, and red dashed lines are the observations.

In principle, this effect should be naturally contained within time-dependent, non-Sobolev simulations of the line-deshadowing instability. However, many uncertainties regarding, e.g., triggering of LDI structure (Sundqvist & Owocki 2013), the treatment of the diffuse force (Owocki & Puls 1999), and multi-dimensional effects (Dessart & Owocki 2003) are present in such *ab-initio* structured wind models. Of particular relevance for the study here, is that the current generation of LDI simulations seems not to properly resolve the internal clump velocity structures, leading to an overprediction of the clump velocity spans δv and to less vorosity than generally needed to reproduce observations (Sundqvist et al. 2010, 2011). Considering these difficulties in creating structured wind models from first principles, we in this section take an alternative approach and examine how vorosity might affect the *global* wind properties mass-loss rate and terminal speed, by implementing the effective opacity formalism developed above into the standard, Sobolev-based, theory of line-driven winds.

4.1. Basic CAK theory

Let us begin by very briefly review the standard CAK (Castor et al. 1975) theory for line driving, cast here in the Gayley (1995) formalism (see also Owocki 2004, for a detailed derivation). For dimensionless line strength $q = \kappa v_{\text{th}} / (\kappa_e c)$ of the line-center mass absorption coefficient κ in units of the electron scattering opacity κ_e , the CAK model assumes a power-law distribution of driving lines,

$$q \frac{dN}{dq} = \frac{1}{\Gamma(\alpha)} \left(\frac{q}{\bar{Q}} \right)^{\alpha-1}, \quad (26)$$

where \bar{Q} is the Gayley (1995) line normalization, α the CAK-power index, and Γ the gamma function.

For a single line of strength q , the line force can be written in terms of the electron scattering acceleration $g_e = \kappa_e F / c$, with radiative flux F , as

$$g_q = q g_e w_{v_0} \frac{1 - e^{-qt_1}}{qt_1}, \quad (27)$$

where $t_1 = \kappa_e \rho c / (dv/dr)$ is the radial Sobolev optical depth for a line with $q = 1$, and $w_{v_0} \equiv v_0 L_v / L$ weights the placement of the line within the luminosity spectrum L_v . As usual in CAK theory we here assume a distribution of driving lines inversely proportional to frequency about the flux maximum, so that $w_{v_0} \approx 1$. The total CAK line force is then obtained by integrating this single line force over the number distribution eqn. 26,

$$g_{\text{cak}} = \int_0^\infty g_q \frac{dN}{dq} dq = \frac{\bar{Q} g_e}{(1 - \alpha)(t_1 \bar{Q})^\alpha}. \quad (28)$$

4.2. Vorosity correction to CAK line force

To correct this for vorosity, we apply the formalism developed in previous sections, and now write the effective opacity of line-strength q for clump optical depth $\tau_{\text{cl}} = t_q / f_{\text{vor}}$ as

$$\frac{q_{\text{eff}}}{q} = \frac{1 + \tau_{\text{cl}} f_{\text{ic}}}{1 + \tau_{\text{cl}}}. \quad (29)$$

Anticipating our following results, we re-write this in terms of the *normalized velocity filling factor* f_{vel} (see previous section), and further neglect a tenuous inter-clump medium $f_{\text{ic}} \ll 1$ on the driving line force, obtaining after re-arranging:

$$q_{\text{eff}} t_1 \approx \frac{f_{\text{vel}} q t_1}{f_{\text{vel}} + (1 - f_{\text{vel}}) q t_1}. \quad (30)$$

Applying q_{eff} instead of q in the second expression of eqn. 28 now gives the vorosity-modified CAK line force.

The evaluation can be most conveniently carried out in terms of a correction factor to the standard CAK force,

$$\frac{g_{\text{vor}}}{g_{\text{cak}}} = \frac{1 - \alpha}{\Gamma(\alpha)} \int_0^\infty \left[1 - \text{Exp} \left(- \frac{f_{\text{vel}} x}{f_{\text{vel}} + (1 - f_{\text{vel}}) x} \right) \right] x^{\alpha-2} dx, \quad (31)$$

where the integration dummy variable $x = q t_1$.

Numerical evaluation of eqn. 31 shows this has the remarkable simple scaling

$$\frac{g_{\text{vor}}}{g_{\text{cak}}} \approx (f_{\text{vel}})^\alpha, \quad (32)$$

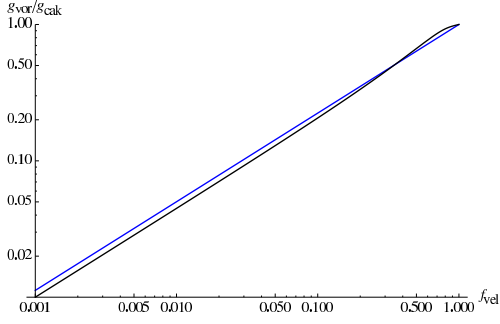


Fig. 7. $g_{\text{vor}}/g_{\text{cak}}$ line forces as functions of f_{vor} , for full numerical integration of the vorosity-modified CAK force eqn. 31 (black) and the simple scaling relation eqn. 32 (blue), for $\alpha = 2/3$.

as shown by Fig. 7, which compares this simple approximation to a full integration of eqn. 31 for $\alpha = 2/3$.

Eqn. 32 thus provides a physically well motivated rationale for studying the global influence of vorosity on line driven winds. For clumping close to the wind base, however, the assumption of neglecting the inter-clump medium’s contribution to the line force might be questionable. But in the absence of good theoretical predictions or reliable diagnostic results for this wind region, we retain throughout this section the assumption of a line force dominated by the dense clumps, also in models involving vorosity in near photospheric layers. This allows us to study the basic physical effects and to derive simple scaling relations.

4.3. Analytic scaling relations for vorosity effect on global wind properties

To provide such an analytic rationale for the effects of vorosity on the global wind parameters mass-loss rate and terminal speed, we consider the steady-state equation of motion for a wind driven by a point source of line radiation, in spherical symmetry and in the zero sound speed limit,

$$v \frac{dv}{dr} = -\frac{GM(1 - \Gamma_e)}{r^2} + g_{\text{cak}}, \quad (33)$$

where $GM(1 - \Gamma_e)/r^2$ is the effective gravitational acceleration for Eddington parameter $\Gamma_e = \kappa_e L / (4\pi GMc)$, and where the radiative line acceleration is assumed to be accurately given by CAK theory. We next introduce the gravitationally scaled inertial acceleration,

$$y' \equiv \frac{r^2 v dv/dr}{GM(1 - \Gamma_e)}, \quad (34)$$

and note that for an inverse radius coordinate $x \equiv 1 - R_*/r$, $y' = dy/dx$ with $y = v^2/v_{\text{esc}}^2$ for effective escape speed v_{esc} reduced by the electron scattering term. This allows us to write the equation of motion in the dimensionless form

$$y' = -1 + C(w')^\alpha, \quad (35)$$

with the constant

$$C \equiv \frac{1}{1 - \alpha} \left(\frac{L}{Mc^2} \right)^\alpha \left(\frac{\bar{Q}\Gamma_e}{1 - \Gamma_e} \right)^{1-\alpha}. \quad (36)$$

Solving eqn. 35 for the tangential intersection between line force and inertia plus gravity now gives the CAK critical solution for the maximal mass-loss rate and wind velocity law $v \propto v_{\text{esc}} \sqrt{x}$

Table 2. Input parameters used in the hydrodynamical wind simulations described in the text.

Parameter	Symbol	Value
Luminosity	L/L_\odot	8.0×10^5
Mass	M/M_\odot	50
Radius	R_*/R_\odot	20
Sound speed	a	23 km/s
CAK power-index	α	0.65, 0.5
Line normalization	\bar{Q}	2000
Electron scattering mass absorption	κ_e	$0.345 \text{ cm}^2/\text{g}$

(see, e.g., Kudritzki et al. 1989; Owocki 2004, for two alternative derivations). More generally though, this point-source model should be corrected for the finite extent of the stellar disc, where

$$f_d(r) = \frac{(1 + \sigma)^{1+\alpha} - (1 + \sigma\mu_\star^2)^{1+\alpha}}{(1 + \alpha)\sigma(1 + \alpha)^\alpha(1 - \mu_\star^2)} \quad (37)$$

for $\mu_\star^2 = 1 - R_\star^2/r^2$ and $\sigma = d \ln v / d \ln r - 1$ is the finite-disc correction factor (Pauldrach et al. 1986; Friend & Abbott 1986) to the CAK line force. Since f_d increases outwards from $r = R_\star$ (to a certain maximum, typically located at $r \sim 1.5R_\star$), the stellar surface now represents a nozzle (“throat”) from which it is hardest to accelerate the material. This fixes the maximal allowed finite-disc mass loss to

$$\dot{M}_{\text{cak}}^{\text{fd}} = \frac{L}{c^2} \frac{\alpha}{(1 + \alpha)^{1/\alpha}(1 - \alpha)} \left(\frac{\bar{Q}\Gamma_e}{1 - \Gamma_e} \right)^{1/\alpha-1}, \quad (38)$$

which is a factor $1/(1 + \alpha)^{1/\alpha}$ lower than the point-source rate. Since the mass loss in such finite-disc models quite generally is set close to the wind base, vorosity starting well above the stellar surface should not affect this scaling. However, if vorosity is important also at low wind radii, the constant setting the maximal mass-loss rate will involve an additional factor, $C \sim 1/f_{\text{vel}}^\alpha$. Due to the scaling $C \sim 1/M^\alpha$ then (eqn. 36), the net effect of velocity-porosity is thus to decrease the mass-loss rate by simply a factor $f_{\text{vel}}(r_{\text{cp}})$, where the velocity filling factor is evaluated at the “critical point” determining this rate.

The wind terminal speed, on the other hand, can be affected also in cases of a vorosity onset radius above this critical point. Considering eqn. 35 for a sudden onset of vorosity in the supersonic $y' \gg 1$ regime, gives the scaling $v/v_{\text{esc}} \propto f_{\text{vel}}^{\alpha/(2-2\alpha)}$, which for a standard $\alpha = 2/3$ results in a linear relation $v \propto f_{\text{vel}}$. While the quantitative speed reduction from such outer wind vorosity, of course, will depend on the exact onset radius, this simple scaling illustrates that the effect on the terminal speed can be quite significant.

4.4. Hydrodynamical wind models with vorosity modified CAK line force

To back up the analytic scaling results above, we next examine effects on mass loss and terminal speed by numerically solving the hydrodynamic conservation equations of mass, momentum, and energy, using the vorosity-corrected CAK line force just developed. This line force is implemented into the hydrodynamics code VH-1 (developed by J. Blondin and collaborators) according to:

$$g_{\text{line}}(r) = g_{\text{cak}}(r) f_d(r) (f_{\text{vel}}(r))^\alpha, \quad (39)$$

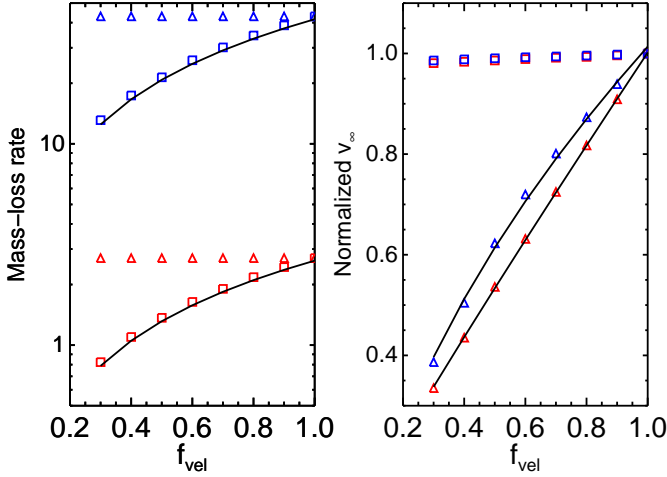


Fig. 8. Mass-loss rates in units of $10^{-6} M_{\odot}/\text{yr}$ (on a logarithmic scale) and terminal speeds in units of v_{∞} in standard, non-vorosity finite-disc models. The triangles and squares denote hydrodynamical calculations (described in text) with vorosity onset radii $r_{\text{vor}} = 1.3 R_{\star} > r_{\text{cp}}$ (triangles) and $r_{\text{vor}} = 1.01 R_{\star} < r_{\text{cp}}$ (squares). Blue symbols assume $\alpha = 0.5$ and red symbols $\alpha = 0.65$. The black solid lines then use the corresponding analytic formulae described in text to predict the mass-loss rate and terminal speed scalings.

where we assume a normalized velocity filling factor

$$f_{\text{vel}}(r) = f_{\text{vel}}^{\infty} + (1 - f_{\text{vel}}^{\infty}) \text{Exp}(-10^3(r/r_{\text{cl}} - 1)); \quad r \geq r_{\text{cl}}, \quad (40)$$

in order to allow for a smooth transition above a vorosity onset radius r_{cl} . To facilitate comparison with the sudden onset of vorosity assumed when deriving the analytic scaling relations, we have inserted a factor 10^3 in the exponential term in eqn. 40, which ensures that the terminal velocity filling factor f_{vel}^{∞} is reached quickly after r_{cl} . Below r_{cl} , f_{vel} is simply set to unity. Using this line force and assuming for simplicity an isothermal wind with sound speed $a = 23 \text{ km/s}$, the hydrodynamical conservation equations are evolved until a stable steady-state wind solution is reached.

For the parameters in Table 2, typical of an early O supergiant in the Galaxy, Fig. 8 compares mass-loss rates in these numerical models with those predicted by the analytic scaling

$$\dot{M}_{\text{vor}} = \dot{M}_{\text{cak}}^{\text{fd}} f_{\text{a}} f_{\text{vel}}(r_{\text{cp}}), \quad (41)$$

where $f_{\text{vel}}(r_{\text{cp}})$ is the normalized velocity filling factor at the critical point determining the mass-loss rate, and where we have also corrected for the finite sound speed a according to the perturbation analysis by Owocki (2004) (see also Appendix A of Owocki & ud-Doula 2004):

$$f_{\text{a}} = 1 + \frac{4\sqrt{1-\alpha}}{\alpha} \frac{a}{v_{\text{esc}}}. \quad (42)$$

The left panel of Fig. 8 reveals very good agreement between the numerical models and this simple analytic scaling formula (within 2-3 %), for both investigated values of the CAK power index α . We note in particular how, indeed, the mass-loss rate is not affected by vorosity with an onset radius above the critical point, which in these finite-disc hydrodynamical simulations lies only a few percent above the stellar surface.

The right panel of Fig. 8 shows the reduction in v_{∞} , and demonstrates the clear anti-correlation between mass loss and terminal speed. When vorosity is important below the critical point, the terminal speed is not affected since the wind then has adjusted to the reduced line force by lowering the mass loading. On the other hand, when vorosity is turned on above this critical point, the wind reacts to the lower line force in the outer parts by reducing its terminal speed by an amount that follows closely the analytic scaling $v_{\infty} \propto (f_{\text{vel}})^{\alpha/(2-2\alpha)}$, as illustrated by the black solid lines in the right panel of the figure.

4.5. Ionization correction

The computations above assume the line driving parameters \bar{Q} and α are constant throughout the wind. To account for potential effects on the wind driving from a radially varying ionization balance, Abbott (1982) introduced another correction factor to the CAK line force, which he took to be $\propto (n_e^{11}/W)^{\delta}$ for electron density n_e measured in units of $10^{11}/\text{cm}^3$, geometric dilution factor W , and ionization power index δ . Since $n_e \propto \rho$, this leads to a new scaling of the line force $\sim 1/\rho^{\alpha-\delta}$ (see eqn. 28), and the corresponding scaling relations for \dot{M} are affected only by a different exponent $\alpha_{\text{eff}} = \alpha - \delta$ (though the absolute values for the predicted rates may change by some additional factors of order unity, see e.g. Pauldrach et al. 1986). But in a clumped stellar wind with negligible inter-clump medium, the electron density has to be evaluated inside the dense clumps, whereby $n_e \propto \langle \rho \rangle / f_{\text{vol}}$ and another factor of $(f_{\text{vol}})^{\delta}$ enters the line force expression. Inserting this into the analysis above then leads to an *upward* correction in the CAK mass-loss rate, by a factor $(1/f_{\text{vol}})^{\delta}$.

We note here these two competing effects from clumping on the line force; whereas the vorosity-associated reduced line force can lead to a *lower* mass-loss rate, the shift in ionization balance stemming from the clumped wind leads to an *increase* in this rate for typical values of δ . In O stars with $\delta \approx 0.1$ (e.g., Pauldrach et al. 1986), the latter results in an upward corrected rate by approximately 25 %, assuming a typical volume filling factor $f_{\text{vol}} \approx 0.1$. Physically, this results from the increased amount of recombination in such clumped models, which drives the ionization balance toward lower ion stages with more efficient driving lines (see also Muijres et al. 2011).

5. Summary and Conclusions

We have developed and benchmarked an effective-opacity formalism for line (and continuum) radiative transfer in accelerating two-component media of (almost) arbitrary density contrasts and clump optical depths. The formalism gives results consistent with our previous, more elaborate models (Sundqvist et al. 2010, 2011), but is simple enough that it can be readily included in the already existing NLTE radiative transfer codes normally used for quantitative modeling and analysis of spectra from hot stars with winds. In addition to the clump volume filling factor f_{vol} , which enters also standard descriptions assuming optically thin clumps, the formalism here is based on two further parameters: f_{ic} , defined as the ratio of the inter-clump density to the mean density, and τ_{cl} , the clump optical depth. Of course, the method can also be used for the case of a negligible inter-clump medium, by simply setting $f_{\text{ic}} = 0$. A crucial point is the calculation of τ_{cl} , which for *continuum* transfer depends on the porosity length h , but for *line* transfer on the velocity clumping factor f_{vor} (see Sect. 2). This difference reflects the physics of the additional leakage of light associated with optically thick clumps in

an accelerating supersonic medium, which for the continuum is set by *spatial* porosity but for lines by porosity in *velocity space* (a.k.a. velocity-porosity, or vorosity).

The effective-opacity law for spectral lines is then incorporated into a vorosity-modified Sobolev with exact integration (vmSEL) method, and used to analyze unsaturated UV wind resonance line doublets. For a given inter-clump density f_{ic} , an analytic investigation shows that in clumped two-component winds, two solutions exist that give identical synthetic line profile doublets. For a given profile-strength ratio between the two individual line components, the two solution branches correspond physically to i) absorption within moderately optically thick clumps with τ_{cl} determined by the blue-to-red profile-strength ratio, and ii) absorption within optically thick clumps ($\tau_{cl} \gg 1$), and the observed profile-strength ratio reproduced by infilling absorption in the inter-clump medium. Direct applications to SiIV in the B supergiant sample of Prinja & Massa (2010) and to PV in the O supergiants ζ Pup and λ Cep demonstrate this severe solution dichotomy. For the B supergiants and ζ Pup the physically more realistic first solution branch gives reasonable mean upward corrections of ~ 5 in mass loss times ion fractions, bringing the PV mass-loss rate for ζ Pup into good agreement with other recent studies focusing on other wavebands than the UV (e.g., Najarro et al. 2011; Hervé et al. 2013; Cohen et al. 2014). The same solution for λ Cep, however, gives only a very modest $\sim 20\%$ upward correction. This would imply a very low mass-loss rate of this star, since it seems unlikely that the PV ion fractions of λ Cep and ζ Pup should be very different. On the other hand, applying the second solution branch and assuming a much higher inter-clump density, $\sim 15\%$ of the mean density, results in a correction factor $\sim 4 - 5$ for also this star; we show that the independent models by Šurlan et al. (2013) indeed correspond to this solution.

In summary, it is very likely that all previous attempts of obtaining mass-loss rates from fitting UV spectra by means of clumped stellar wind models – including our own – suffer from the uniqueness problem found in this paper (e.g., Oskinova et al. 2007; Sundqvist et al. 2011; Šurlan et al. 2013). Empirically it seems possible to break these degeneracies only by a real multi-diagnostic study, in which several diagnostics are considered simultaneously. In particular, X-ray absorption is a very promising mass-loss indicator (Cohen et al. 2010, 2011; Hervé et al. 2013; Cohen et al. 2014), since it has been shown that this diagnostic seems to be free of most issues associated with wind clumping (Sundqvist et al. 2012a; Hervé et al. 2013; Leutenegger et al. 2013). Another interesting possibility is to target stars with very dense winds, like Wolf-Rayet stars or Luminous Blue Variables in their quiet stage, where effects should be larger and additional diagnostics are available (for example electron scattering wings, which are too weak to be of diagnostic value in the OB-star winds studied here).

Of course, to some extent these degeneracies are artefacts of present-day diagnostic models, which treat clumping by using a set of adjustable input parameters rather than computing clumping properties from first principles. In an ideal situation, one would instead use simulations of the structured wind to quantitatively predict, e.g., vorosity and inter-clump medium properties. However, as discussed in previous sections, presently such predictions are quantitatively very uncertain. For example, the relatively dense inter-clump medium in the highly supersonic wind indicated by the second branch solutions discussed above ($f_{ic} > 0.1$), is inconsistent with basic predictions of the fundamental, inherent instability of line-driving (e.g., Owocki et al. 1988; Feldmeier 1995; Owocki & Puls 1996;

Sundqvist & Owocki 2013) that is the likely cause of clumping in this wind region, and which predicts much lower inter-clump densities.

We next incorporated the effective-opacity formalism also into the standard CAK theory of line-driven winds, showing that vorosity leads to a reduced line force scaling simply with the normalized velocity filling factor $f_{vel} \equiv f_{vor}/(1 + f_{vor})$ as f_{vel}^α , for CAK power index α . By analytic and numerical hydrodynamics calculations, we then derived scaling relations for the anti-correlated behavior of the global wind parameters mass-loss rate and terminal speed: For vorosity starting below the wind “critical point”, the mass-loss rate is reduced by factor of f_{vel} but the terminal speed remains unaffected, whereas for vorosity starting above this critical point the mass-loss rate is unaffected but the terminal speed reduced by $v_\infty \propto f_{vel}^{\alpha/(2-2\alpha)}$. We finally also provide a simple correction factor accounting for the expected shift in ionization in a clumped wind, which for a negligible inter-clump medium scales as $\dot{M} \propto (1/f_{vor})^\delta$, with Abbott’s ionization parameter δ (≈ 0.1 for a typical O star wind).

These analytic scalings are qualitatively consistent with the numerical simulations by Muijres et al. (2011), who modeled the effects of clumping and porosity in velocity space by using a smooth wind velocity law and assigning clump length scales⁵ l , and found general trends of higher mass-loss rates from the shifted ionization balance and lower rates from the inclusion of velocity porosity. A detailed comparison is not possible, however, since their Monte-Carlo models only predict the total wind kinetic energy $\dot{M}v_\infty^2$, and so cannot separate between a change in terminal wind speed and a change in mass-loss rate.

The upshot from the study here is thus that while vorosity generally gives an *upward* correction in empirical mass-loss rates derived from spectral fitting (true for all diagnostics, when compared to models assuming optically thin clumps), it could also, if there is substantial vorosity at the wind critical point, cause a *downward* correction in mass-loss rates predicted by line-driven wind theory.

Such downward corrections would be consistent with the recent empirical mass-loss determination of nearby, bright O-stars by Cohen et al. (2014) (using presumably clumping-insensitive X-ray diagnostics), who find rates that are on average a factor of ~ 3 lower than current theoretical predictions, and also with the many observational (e.g., Lépine & Moffat 2008; Puls et al. 2006; Bouret et al. 2012; Cohen et al. 2014) and theoretical (Sundqvist & Owocki 2013) findings that strongly indicate clumping in near photospheric layers. A reduced line force would further help explain also the long-standing problem of winds from late-type O main-sequence stars, which seem to be much weaker than predicted by standard theory (see overview in Puls et al. 2008).

Future papers in this series will i) develop more refined theoretical wind models to account quantitatively for the velocity-porosity effect, and ii) employ the effective-opacity formalism developed in this paper in multi-wavelength, multi-diagnostic NLTE studies of hot star winds in an attempt to break the severe degeneracies discussed above.

6. Appendix A

Let us consider a two-component ($i = 1, 2$) mixture described by homogeneous Markovian statistics, with spatially constant

⁵ More precisely, they assigned overdensities of clumps C_c and mean separations L , giving clump length scales $l \sim L/C_c^{1/3}$ and clump velocity spans $\delta v \sim (dv/ds)l$, along path length s .

opacities χ_i and probabilities $p_i = \lambda_i/(\lambda_1 + \lambda_2)$ of at any given point along a ray being in component i , where λ_i is the mean chord length of material i . In this scenario, the stochastic radiative transfer equation can be solved analytically for the mean intensity $\langle I \rangle$ (e.g., Levermore et al. 1986). The book by Pomraning (1991) provides the full derivation; here we merely give the result, along with a translation of the parameters used by Pomraning and collaborators to those used in this paper.

The result for the averaged intensity at a distance s along a ray is

$$\langle I \rangle = \left(\frac{r_+ - \hat{\sigma}}{r_+ - r_-} \right) e^{-r_+ s} + \left(\frac{\hat{\sigma} - r_-}{r_+ - r_-} \right) e^{-r_- s}, \quad (43)$$

with

$$2r_{\pm} = \langle \chi \rangle + \hat{\sigma} \pm \sqrt{(\langle \chi \rangle - \hat{\sigma})^2 + 4\beta_M}, \quad (44)$$

$$\hat{\sigma} = p_1 \chi_2 + p_2 \chi_1 + \frac{1}{\lambda_2} + \frac{1}{\lambda_1}, \quad (45)$$

$$\beta_M = (\chi_2 - \chi_1)^2 p_2 p_1, \quad (46)$$

and average opacity $\langle \chi \rangle \equiv \chi_1 p_1 + \chi_2 p_2$.

Assuming clumps to be component 1, we follow the arguments by Sundqvist et al. (2012a) and identify $f_{\text{vol}} = p_1$, $(1 - f_{\text{vol}}) = p_2$ (see also Pomraning 1991), $p_2 \lambda_2 = h$, and finally $\chi_1 = \chi_{\text{cl}}$ and $\chi_2 = \chi_{\text{ic}}$. As demonstrated by the left panel of Fig. 1, these identifications indeed give perfect agreement for the effective opacity $\chi_{\text{eff}} = -\ln \langle I \rangle / s$ when compared to the numerical 3D box experiments in Sect. 2.

We note further that also Pomraning (1991), by means of a mean-free path argument, derives an ‘‘effective opacity’’ approximation for their two-component model:

$$\chi_{\text{eff}}^{\text{Pom}} = \frac{\langle \chi \rangle + \chi_1 \chi_2 \ell_c}{1 + (p_1 \chi_2 + p_2 \chi_1) \ell_c}, \quad (47)$$

with correlation length $\ell_c = \lambda_1 \lambda_2 / (\lambda_1 + \lambda_2)$. Translated to the notation used in this paper, eqn. 47 becomes

$$\frac{\chi_{\text{eff}}^{\text{Pom}}}{\langle \chi \rangle} = \frac{1 + f_{\text{ic}} \tau_{\text{cl}} (1 - f_{\text{vol}})}{1 + \tau_{\text{cl}} (1 + \frac{f_{\text{vol}} \chi_{\text{ic}}}{(1 - f_{\text{vol}}) \chi_{\text{cl}}})}, \quad (48)$$

assuming here $\chi_{\text{ic}} / \langle \chi \rangle = f_{\text{ic}}$. In the limit of $f_{\text{vol}} \ll 1$ (for $\chi_{\text{ic}} \leq \chi_{\text{cl}}$), eqn. 48 simplifies to the effective-opacity law adopted in Sect. 2:

$$\frac{\chi_{\text{eff}}^{\text{Pom}}}{\langle \chi \rangle} \approx \frac{1 + f_{\text{ic}} \tau_{\text{cl}}}{1 + \tau_{\text{cl}}} = \frac{\chi_{\text{eff}}^{\text{SPO}}}{\langle \chi \rangle}. \quad (49)$$

Testing has shown that this simple bridging law for approximating the effective opacity actually reproduces the analytic and the numerical intensity test-calculations in Sect. 2 somewhat *better* than the more complicated one suggested by Levermore and Pomraning (eqn. 47). In particular, eqn. 49 also represents a very simple extension of an ‘‘intuitive’’ law that corrects the clump+void model (see Sect. 2) by simply adding a tenuous inter-clump medium with $f_{\text{ic}} \ll 1$:

$$\frac{\chi_{\text{eff}}}{\langle \chi \rangle} \approx \frac{1}{1 + \tau_{\text{cl}}} + f_{\text{ic}} = \frac{1 + \tau_{\text{cl}} f_{\text{ic}} + f_{\text{ic}}}{1 + \tau_{\text{cl}}}. \quad (50)$$

In contrast to this expression though, the effective opacity law used in this paper (obtained by simply dropping the alone-standing f_{ic} term in the last expression of eqn. 50) also preserves the ‘‘smooth’’ medium limit $\chi_{\text{eff}} = \langle \chi \rangle$ for $f_{\text{ic}} = 1$.

Acknowledgements. JOS gratefully acknowledges support from DFG grant Pu117/8-1. J.O.S. and J.P. also acknowledge the help from the International Space Science Institute at Bern, Switzerland. We thank John Hillier and the anonymous referee for useful comments on the manuscript.

References

- Abbott, D. C. 1982, *ApJ*, 259, 282
 Bouret, J.-C., Hillier, D. J., Lanz, T., & Fullerton, A. W. 2012, *A&A*, 544, A67
 Castor, J. I., Abbott, D. C., & Klein, R. I. 1975, *ApJ*, 195, 157
 Cohen, D. H., Gagné, M., Leutenegger, M. A., et al. 2011, *MNRAS*, 415, 3354
 Cohen, D. H., Leutenegger, M. A., Wollman, E. E., et al. 2010, *MNRAS*, 405, 2391
 Cohen, D. H., Wollman, E. E., Leutenegger, M. A., et al. 2014, *MNRAS*, 439, 908
 Dessart, L. & Owocki, S. P. 2003, *A&A*, 406, L1
 Feldmeier, A. 1995, *A&A*, 299, 523
 Feldmeier, A., Oskinova, L., & Hamann, W.-R. 2003, *A&A*, 403, 217
 Friend, D. B. & Abbott, D. C. 1986, *ApJ*, 311, 701
 Fullerton, A. W., Massa, D. L., & Prinja, R. K. 2006, *ApJ*, 637, 1025
 Gayley, K. G. 1995, *ApJ*, 454, 410
 Gräfener, G., Owocki, S. P., & Vink, J. S. 2012, *A&A*, 538, A40
 Gräfener, G. & Vink, J. S. 2013, *A&A*, 560, A6
 Hamann, W.-R. 1981, *A&A*, 93, 353
 Hamann, W.-R., Feldmeier, A., & Oskinova, L. M., eds. 2008, *Clumping in hot-star winds*, Universitätsverlag Potsdam 2008
 Hervé, A., Rauw, G., & Nazé, Y. 2013, *A&A*, 551, A83
 Hillier, D. J. 1991, *A&A*, 247, 455
 Hillier, D. J. 2008, in *Clumping in Hot-Star Winds*, ed. W.-R. Hamann, A. Feldmeier, & L. M. Oskinova, 93–+
 Kudritzki, R.-P., Pauldrach, A., Puls, J., & Abbott, D. C. 1989, *A&A*, 219, 205
 Lamers, H. J. G. L. M., Cerruti-Sola, M., & Perinotto, M. 1987, *ApJ*, 314, 726
 Lépine, S. & Moffat, A. F. J. 2008, *AJ*, 136, 548
 Leutenegger, M. A., Cohen, D. H., Sundqvist, J. O., & Owocki, S. P. 2013, *ApJ*, 770, 80
 Levermore, C. D., Pomraning, G. C., Sanzo, D. L., & Wong, J. 1986, *Journal of Mathematical Physics*, 27, 2526
 Lucy, L. B. 1984, *ApJ*, 284, 351
 Massa, D. L., Prinja, R. K., & Fullerton, A. W. 2008, in *Clumping in Hot-Star Winds*, ed. W.-R. Hamann, A. Feldmeier, & L. M. Oskinova, 147, Universitätsverlag Potsdam 2008
 Muijres, L. E., de Koter, A., Vink, J. S., et al. 2011, *A&A*, 526, A32
 Najarro, F., Hanson, M. M., & Puls, J. 2011, *A&A*, 535, A32
 Oskinova, L. M., Hamann, W.-R., & Feldmeier, A. 2007, *A&A*, 476, 1331
 Owocki, S. 2004, in *EAS Publications Series*, Vol. 13, *EAS Publications Series*, ed. M. Heydari-Malayeri, P. Stee, & J.-P. Zahn, 163–250
 Owocki, S. P. 2008, in *Clumping in Hot-Star Winds*, ed. W.-R. Hamann, A. Feldmeier, & L. M. Oskinova, 121–
 Owocki, S. P., Castor, J. I., & Rybicki, G. B. 1988, *ApJ*, 335, 914
 Owocki, S. P. & Cohen, D. H. 2006, *ApJ*, 648, 565
 Owocki, S. P., Gayley, K. G., & Shaviv, N. J. 2004, *ApJ*, 616, 525
 Owocki, S. P. & Puls, J. 1996, *ApJ*, 462, 894
 Owocki, S. P. & Puls, J. 1999, *ApJ*, 510, 355
 Owocki, S. P. & Rybicki, G. B. 1984, *ApJ*, 284, 337
 Owocki, S. P. & Rybicki, G. B. 1985, *ApJ*, 299, 265
 Owocki, S. P. & ud-Doula, A. 2004, *ApJ*, 600, 1004
 Pauldrach, A., Puls, J., & Kudritzki, R. P. 1986, *A&A*, 164, 86
 Pomraning, G. C. 1991, *Linear kinetic theory and particle transport in stochastic mixtures*, ed. Pomraning, G. C., New Jersey: World Scientific, c1991, Series on advances in mathematics for applied sciences, v. 7
 Prinja, R. K. & Massa, D. L. 2010, *A&A*, 521, L55
 Prinja, R. K. & Massa, D. L. 2013, *A&A*, 559, A15
 Puls, J., Markova, N., Scuderi, S., et al. 2006, *A&A*, 454, 625
 Puls, J., Owocki, S. P., & Fullerton, A. W. 1993, *A&A*, 279, 457
 Puls, J., Urbaneja, M. A., Venero, R., et al. 2005, *A&A*, 435, 669
 Puls, J., Vink, J. S., & Najarro, F. 2008, *A&A Rev.*, 16, 209
 Sundqvist, J. O. & Owocki, S. P. 2013, *MNRAS*, 428, 1837
 Sundqvist, J. O., Owocki, S. P., Cohen, D. H., Leutenegger, M. A., & Townsend, R. H. D. 2012a, *MNRAS*, 420, 1553
 Sundqvist, J. O., Owocki, S. P., & Puls, J. 2012b, in *Astronomical Society of the Pacific Conference Series*, Vol. 465, *Proceedings of a Scientific Meeting in Honor of Anthony F. J. Moffat*, ed. L. Drissen, C. Rubert, N. St-Louis, & A. F. J. Moffat, 119
 Sundqvist, J. O., Puls, J., & Feldmeier, A. 2010, *A&A*, 510, 11
 Sundqvist, J. O., Puls, J., Feldmeier, A., & Owocki, S. P. 2011, *A&A*, 528, 64
 Šurlan, B., Hamann, W.-R., Aret, A., et al. 2013, *A&A*, 559, A130
 Šurlan, B., Hamann, W.-R., Kubát, J., Oskinova, L. M., & Feldmeier, A. 2012, *A&A*, 541, A37
 Zsargó, J., Hillier, D. J., Bouret, J.-C., et al. 2008, *ApJ*, 685, L149